Bull. Mater. Sci., Vol. 37, No. 3, May 2014, pp. 541–547. © Indian Academy of Sciences.

Structural, optical and magnetic properties of cobalt-doped CdSe nanoparticles

JASPAL SINGH* and N K VERMA

Nano Research Lab, School of Physics and Materials Science, Thapar University, Patiala 147 004, India

MS received 19 October 2012; revised 8 December 2012

Abstract. Pure and Co-doped CdSe nanoparticles have been synthesized by hydrothermal technique. The synthesized nanoparticles have been characterized using X-ray diffraction (XRD), ultraviolet-visible spectroscopy (UV–Visible), photoluminescence spectroscopy (PL), energy dispersive spectroscopy (EDS), transmission electron microscopy (TEM) and superconducting quantum interference device (SQUID), at room temperature. From XRD analysis, pure and cobalt-doped CdSe nanoparticles have been found to be polycrystalline in nature and possess zinc blende phase having cubic structure. In addition to this, some peaks related to secondary phase or impurities such as cobalt diselenide ($CoSe_2$) have also been observed. The calculated average crystallite size of the nanoparticles lies in the range, 3–21 nm, which is consistent with the results obtained from TEM analysis. The decrease in average crystallite size and blue shift in the band gap has been observed with Co-doping into the host CdSe nanoparticles. The magnetic analysis shows the ferromagnetic behaviour up to 10% of Co-doping concentration. The increase of Co content beyond 10% doping concentration leads to antiferromagnetic interactions between the Co ions, which suppress the ferromagnetism.

Keywords. Nanoparticles; dilute magnetic semiconductor; ferromagnetism.

1. Introduction

Dilute magnetic semiconductors (DMS) are the materials in which a part of the host lattice is replaced by substitutional magnetic ions (transitions or rare earth metal ions). DMS exhibits *sp–d* exchange interactions between dopant (magnetic ions) and the host semiconductor; this may result in large Zeeman splitting, giant Faraday rotation, anomalous Hall effect and spin glass behaviour (Furdyna 1982; Toyosaki *et al* 2004; Yu *et al* 2010). These materials are very promising for spintronic applications, wherein they allow the manipulation of carrier spins in semiconductors. In spin-based electronic devices, the simultaneous use of both the charge and spin to transport, store and process information leads to enhanced non-volatile memory, speed, integration density and low power consumption. Spin light-emitting diodes have been demonstrated at cryogenic temperatures using II–VI- and III–V-based DMS materials, thereby limiting their use at room temperature (Stroud *et al* 2002). So, for practical applications these materials must possess Curie temperature (T_c), at or above the room temperature, which is till date a challenging task. Numerous reports have been published with conflicting results on the origin and observation of room temperature ferromagnetism in DMS materials (Pearton *et al* 2004; Seehra *et al* 2008; Dietl 2010; Santara *et al* 2011; Xu *et al* 2012).

In DMS of II–VI semiconductor materials, magnetic coupling has been observed between the *p*-valence band electrons of host and *d*-orbitals of transition metal (Fe, Mn and Co). But, considerable interest has been focused on Co-doped systems, as Co^{2+} ($3d^7$) exists in a singlet ground state having tetrahedral coordination environment and is easily introduced into host II–VI semiconducting material (Ladizhansky *et al* 1997). The magnetic behaviour of Co^{2+} doped DMS-based alloys is determined from the nature of its ground state. In free state, Co^{2+} ions exhibit singlet ground state (4F) and shows paramagnetism, however, when it becomes part of host (semiconductor, e.g. CdSe), its singlet state split into three multiple-states because of crystal filed and spin orbit interactions, and this govern its magnetic nature (Bartholomew *et al* 1989; Isber *et al* 2001). However, Co-doped II–VI DMS based alloys shows antiferromagnetic interactions due to stronger coupling between cobalt *d*-orbitals and conduction band of the host II–VI semiconducting material as compared to their Mn counterpart (Lewicki *et al* 1989; Hamdani *et al* 1992).

CdSe nanoparticles-based DMS are very promising for applications in solar cells (Murray *et al* 1993), biological labelling (Bruchez Jr *et al* 1998), spintronic devices (Beaulac *et al* 2008). However, limited reports are available on the cobalt-doped CdSe nanoparticles as a DMS

*Author for correspondence (jaspal0314@gmail.com)

material. The antiferromagnetism has been observed in bulk Co-doped CdSe (Niu *et al* 1989). However, paramagnetism and spin glass (SG) behaviour has been observed in Co-doped CdSe quantum dots at very low temperature (Hanif *et al* 2002). Further, the direct *sp–d* exchange interactions have been observed in Co-doped CdSe quantum dots, which is a significant feature of DMS material (Archer *et al* 2007).

The present work aims at the synthesis of Co-doped CdSe nanoparticles and, investigations of their optical, structural and magnetic properties.

2. Experimental

Pure and Co-doped CdSe nanoparticles with cobalt concentration of 5, 10 and 15% were synthesized following a little modification in previously reported procedure (Singh and Verma 2012). In the typical synthesis procedure, stoichiometric amount of cadmium chloride tetrahydrate ($CdCl_2{\cdot}4H_2O$) and cobaltous chloride hexahydrate ($CoCl_2{\cdot}6H_2O$) were dissolved in de-ionized water. Sodium dodecyl sulfate (SDS) was used as a surfactant in the reaction. Further, separately prepared solution of selenium (Se) reduced with hydrazine hydrate was added to the above solution. The as-obtained mixture was transferred to 50 mL teflon-lined autoclave which was then placed for 10 h at 180 °C in a heating oven. The precipitates were washed several times with distilled water and ethanol, finally were dried in hot air oven at 60 °C to obtain the powder.

XRD data of the synthesized nanoparticles was recorded in order to identify the phase purity and structure using PANalytical X'Pert PRO X-ray diffractometer with CuK_α ($\lambda = 1{\cdot}5418$ Å) operated at 45 kV and 40 mA. Morphology of the nanoparticles was observed from TEM (Hitachi H-7500). EDS measurements were carried out using Oxford analytical system attached with SEM, which is the direct evidence of the presence of Co in the host nanoparticles. Optical absorption, emission spectra were studied with UV–Visible (Analytic Jena, SPECORD 205) spectrophotometer and PL (Perkin Elmer LS55 spectrofluorimeter). Magnetic field hysteresis (*M–H*) was performed by SQUID (Quantum Design).

3. Results and discussion

3.1 *XRD analysis*

The structure, phase purity and crystallite size of the nanoparticles were determined from the XRD pattern, as shown in figure 1. All the diffraction peaks corresponding to pure CdSe nanoparticles have been found to be in good agreement with standard JCPDS card no. 19-0191, depicting the formation of zinc blende phase with cubic structure. The diffraction peaks at 2θ (degree) values of 25·40, 42·02 and 49·84 correspond to (111), (220) and (311) planes of cubic CdSe, respectively. The extra peaks observed at 2θ (degree), 34·43 and 45·92 in all the doped samples are related to cobalt diselenide ($CoSe_2$) (JCPDS card no. 09-0234). Considerable peak broadening has been observed with Co-doping concentration which indicates the incorporation of Co in the host CdSe nanoparticles. The lower ionic radius of Co^{2+} (0·72 Å) ions as compared to Cd^{2+} (0·97 Å) ions, generates compressive strain in the host nanoparticles leading to peak broadening in XRD pattern. The peak broadening in XRD patterns may arise due to several other reasons such as smaller crystallite size, instrumental error and fast scanning (Cullity 1978). As in the present case, proper precautions have been taken into account during scanning such as instrument calibration with standard samples and slow scan rate. Therefore, the observed broadening (figure 1) is due to the strain and smaller crystallite size, where their contribution to peak broadening is independent of each other. Therefore, total broadening can be written as sum of these two as $\beta_{\text{total}} = \beta_{\text{strain}} + \beta_{\text{crystallite size}}$ and can be calculated using Williamson–Hall (W–H) equation (Williamson and Hall 1953):

$$\beta_{\text{total}} \cos\theta/\lambda = 1/d + \eta \sin\theta/\lambda,$$

where η is the effective strain present in the material, d the effective crystallite size, λ the wavelength of X-ray radiation, β the full width at half maxima and θ the diffraction angle. Negative slopes of pure and Co-doped CdSe nanoparticles as shown in figure 2 indicate the presence of effective compressive strain in the crystal lattice. Table 1 shows the calculated values of strain, crystallite sizes from XRD and TEM. The higher magnitude of the slope with the incorporation of Co in CdSe suggests enhancement in the strain and reduction in the crystallite size.

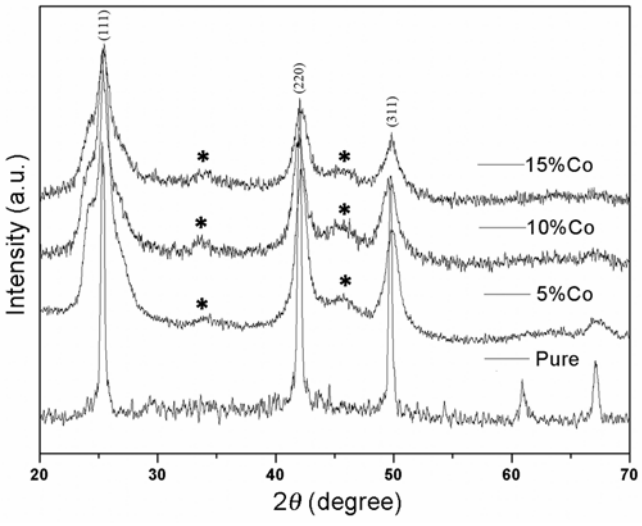

Figure 1. XRD pattern of pure, 5, 10 and 15% Co-doped CdSe nanoparticles.

Table 1. Calculated values of average crystallite size, average particle size and strain of pure and Co-doped CdSe nanoparticles.

Co content (wt%)	Average crystallite size from XRD d (nm)	Average particle size from TEM (nm)	Strain, η
0	20·7	41·2	0·00537
5	3·8	9·5	0·03769
10	3·6	8·9	0·04933
15	3·1	7·5	0·05988

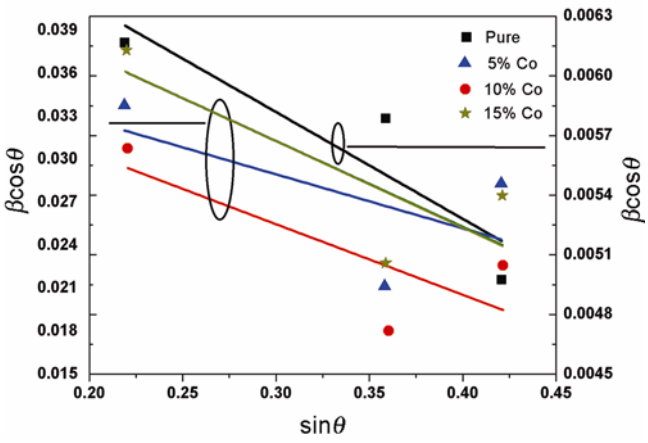

Figure 2. W–H plot for pure and Co-doped CdSe nanoparticles.

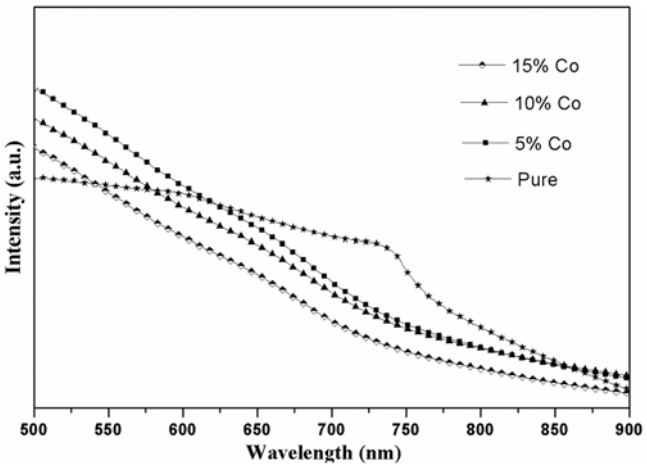

Figure 3. UV–Visible absorption spectra of pure and Co-doped CdSe nanoparticles.

3.2 *UV-Visible spectroscopy*

Figure 3 shows the UV-Visible absorption spectra of pure and Co-doped CdSe nanoparticles. The bulk CdSe has a band gap of 1·72 eV corresponding to the absorption wavelength of 714 nm. In the present system, the pure CdSe nanoparticles show red shift, which is due to the band narrowing effect arising from the strained anisotropic structure, as well as the scattering of light in different directions (Jin *et al* 2011). A long tail in UV–Visible spectrum has also been observed in pure CdSe nanoparticles, which indicates the formation of faceted or rod like structures (Limaye *et al* 2011). However, with Co-doping the blue shift has been observed. This can be explained by quantum confinement of electron–hole pairs (excitons), which is dominant when the particle size is less than or comparable to the Bohr exciton radius of the bulk material. The Bohr exciton radius of CdSe is around 5·5 nm (Ekimov *et al* 1993). Hence, CdSe nanoparticles of radii $\leq 5{\cdot}5$ nm show quantum confinement effect with absorbance maxima shifted to the shorter wavelengths. The energy band gap (E_g) of the synthesized nanoparticles have been calculated using second-order derivative of the absorption spectra (figure 4) and it comes out to be 1·65, 1·78, 1·80 and 1·83 eV for pure, 5, 10 and 15%, respectively. The E_g value has been found to increase with Co-doping concentration which can be attributed to decrease in particle size.

3.3 *Photoluminescence study*

PL emission spectra of pure and Co-doped CdSe nanoparticles have been recorded at room temperature with excitation wavelength of 480 nm as shown in figure 5. Two broad emission peaks, at 576 and 632 nm, have been observed in the emission spectrum. The weak emission peak at 576 nm related to deep trap levels and strong emission peak at 632 nm is due to shallow region trapped electron–hole pairs (Bawendi *et al* 1992). The emission from deep trap levels does not change with doping because it is independent of particle size and doping concentration, whereas emission from shallow traps decreases with Co-doping concentration (Hasanzadeh and Shayesteh 2011). Co acts as electron trapping centre, which leads to non-radiative recombinations. So, it is concluded that Co acts as a quencher impurity in the host CdSe nanoparticles.

3.4 *Energy dispersive X-ray analysis*

The compositional analysis has been done using EDS in order to confirm the elements and quantify their percentage composition as shown in figure 6. The peaks of cad-

mium (Cd), cobalt (Co) and selenium (Se) have been observed, which confirm the presence of Co in the host CdSe nanoparticles. EDS measurement reveals 5·24, 10·03 and 14·80% Co for 5, 10 and 15% doping concentration, consistent with the weight percent of Co added. Also, no traces of any other impurity elements have been observed in the samples.

3.5 *Transmission electron microscopy (TEM)*

From figure 7, it is clear that pure CdSe nanoparticles exhibit a mixed morphology of spherical, faceted and rod-shaped. Further, doping of Co leads to spherical CdSe nanoparticles with decreased particle size. The shape of nanocrystals depends on the concentration of the initial precursors and growth kinetics (Peng *et al* 1998; Wang *et al* 2006). At high monomer concentration, growth rate of nanocrystals is fast, leading to the formation of different shapes. The doping of Co into CdSe nanoparticles limits the growth rate in the solution growth process and this favours the formation of spherical nanoparticles having smaller particle size under these slow growth conditions (Hays *et al* 2005; Sambasivam *et al* 2009). The average particle size of pure, 5, 10 and 15% Co-doped CdSe nanoparticles has been found to be 41·2, 9·5, 8·9 and 7·5 nm, respectively. Particle size from TEM is consistent with the results obtained from XRD, the irregular shaped nanoparticles for pure CdSe further support the long tail in UV–Visible spectra.

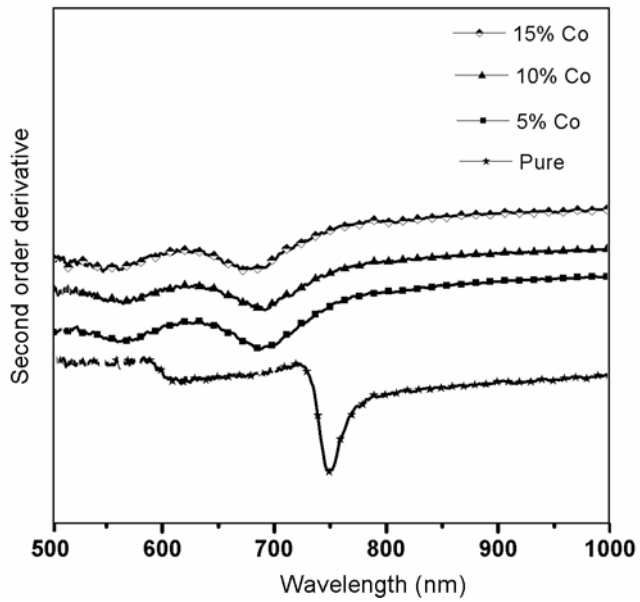

Figure 4. Second-order derivative of absorption spectra of pure and Co-doped CdSe nanoparticles.

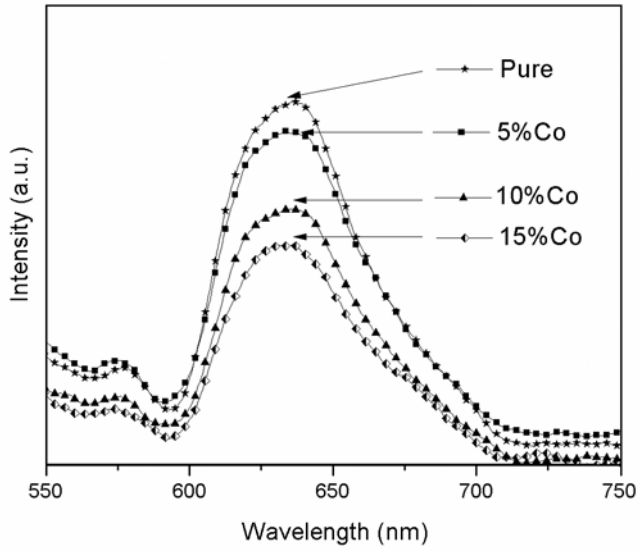

Figure 5. Room temperature PL spectra of pure and Co-doped CdSe nanoparticles recorded at an excitation wavelength of 480 nm.

3.6 *Magnetic analysis*

Figure 8 shows the magnetization vs applied magnetic field hysteresis (M–H) loops of pure and Co-doped CdSe nanoparticles at room temperature. Hysteresis curves with coercivity (H_c) and remanence magnetization (M_r) values, 221, 301, 99, 65 Oe and $2{\cdot}83 \times 10^{-4}$, $6{\cdot}15 \times 10^{-5}$, $2{\cdot}93 \times 10^{-4}$, $5{\cdot}23 \times 10^{-4}$ emu/g, respectively, have been observed for pure, 5, 10 and 15% of doping concentration. For pure CdSe nanoparticles, diamagnetic curve (figure 8(a)) has been obtained, as expected from its intrinsic diamagnetic nature. At a lower magnetic field value, as shown in inset of figure 8(a), weak ferromagnetism has been observed, which may be attributed to the charge transfer between capping agent and host CdSe nanoparticles (Meulenberg *et al* 2009). However, the universality of ferromagnetism has been observed in CdSe nanoparticles (Sundaresan and Rao 2009). The magnetism in doped CdSe nanoparticles may be originated possibly from carrier mediated exchange interactions between delocalized carriers of the host and the localized d spins of the Co ions (Singh *et al* 2008; Saravanan *et al* 2011). The secondary phase of $CoSe_2$ does not contribute to observed magnetism in present system but it shows paramagnetism below 4 K (Furuseth and Kjekshus 1969). Also, the origin of observed magnetism in doped CdSe nanoparticles may be attributed to the presence of secondary impurities or phases such as Co_3Se_4, Co_7Se_8 and Co_9Se_8 (Hayashi *et al* 1986; Ikeda *et al* 1995; Zhang *et al* 2012). The S-type hysteresis loop has been observed in 5% Co-doping concentration, which shows the emergence of ferromagnetism in the host nanoparticles. Further, the diamagnetic contribution arises from the host, which reduces the magnetic moment at higher magnetic field. With increase in doping concentration up to 10%, the ferromagnetic behaviour has been observed with weak magnetic moment (figure 8(c)), which may be due to the

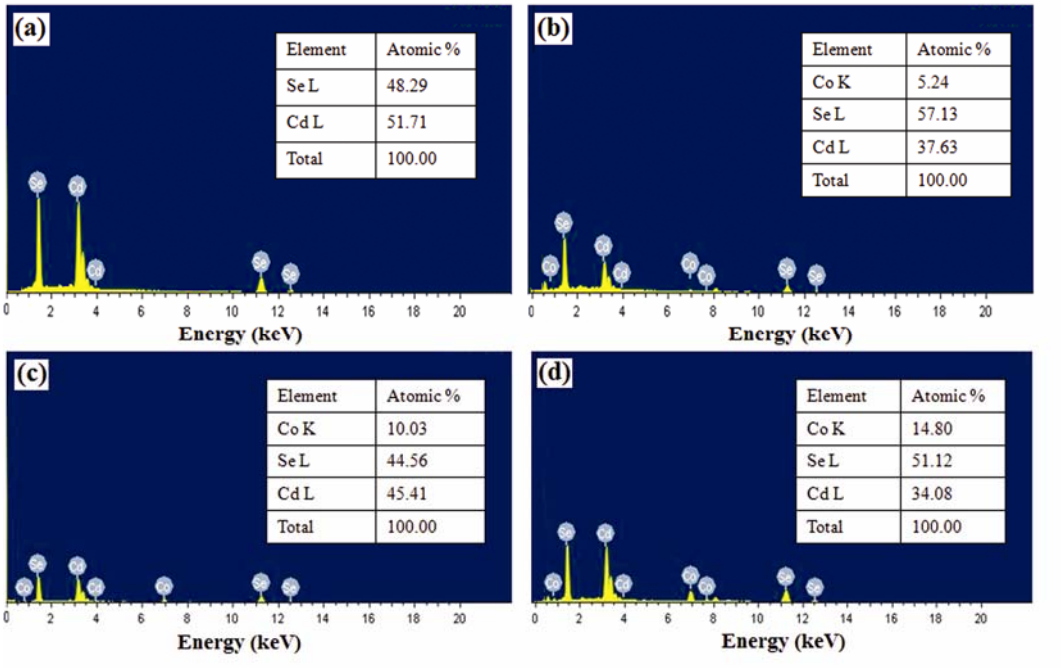

Figure 6. EDS spectrum of (**a**) pure, (**b**) 5, (**c**) 10 and (**d**) 15% Co-doped CdSe nanoparticles.

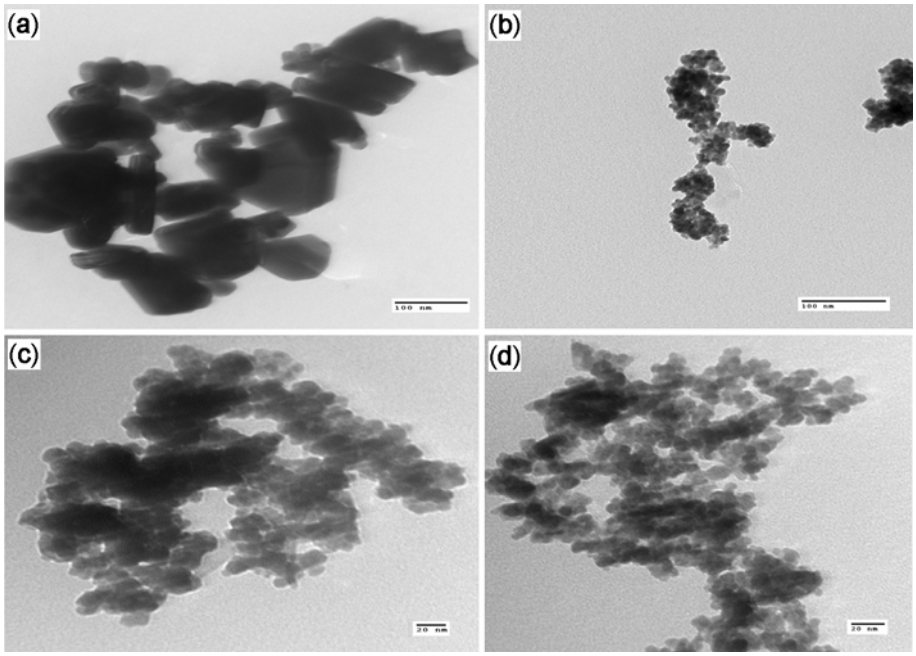

Figure 7. TEM micrographs of samples with (**a**) pure, (**b**) 5, (**c**) 10 and (**d**) 15% Co-doping concentration.

long range ferromagnetic ordering in Co-doped CdSe nanoparticles. The ferromagnetic loop is not saturated, but noticeable H_c and M_r values have been observed for 10% of Co-doping. Further, the increase of Co content beyond 10% led to linearization of *M–H* hysteresis curve (figure 8(d)). It indicates that Co–Co superexchange interaction dominates at higher Co-doping concentration, thereby possesses antiferromagnetic character. Hanif *et al* (2002) and Archer *et al* (2007) reported similar results; the Co-doped CdSe nanoparticles show antiferromagnetic behaviour, due to strong *sp–d* exchange interaction between Co *d*-orbitals and conduction band of the host CdSe. The exact origin of magnetism still not clear and further studies may be required.

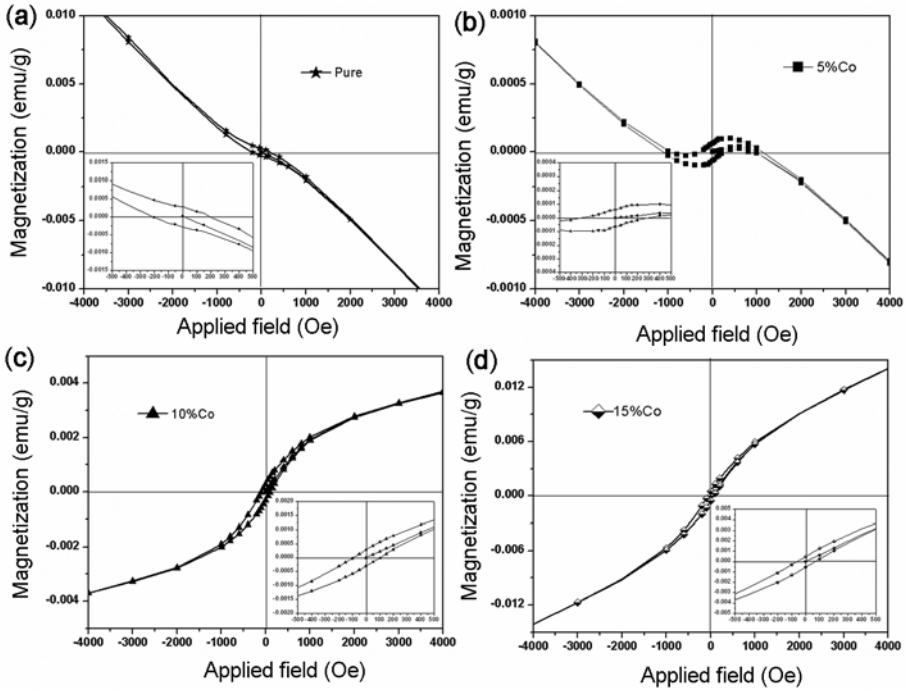

Figure 8. *M–H* curves showing hysteresis of (**a**) pure, (**b**) 5, (**c**) 10 and (**d**) 15 Co-doping concentration. Inset shows enlarged view of *M–H* curve.

4. Conclusions

Our investigations on hydrothermally-synthesized pure and Co-doped CdSe nanoparticles reveal that the dopant concentration causes distinctive changes in the structural, optical, morphological and magnetic properties of CdSe nanoparticles. Pure CdSe nanoparticles possess polycrystalline cubic structure; whereas the additional peaks of cobalt diselenide ($CoSe_2$) have been observed due to Co-doping. The blue shift and luminescence quenching with doping concentration indicates the presence of Co ions in CdSe nanoparticles. From TEM analysis, it has been observed that the pure CdSe nanoparticles formed were of irregular shapes, whereas Co-doping results in spherical morphology with decreased particle size. The *M–H* analysis reveals the transformation of diamagnetic pure CdSe nanoparticles to ferromagnetic Co-doped nanoparticles at lower doping concentrations. However, further increase in Co doping has led to antiferromagnetism in the host nanoparticles. The transition from ferromagnetism to antiferromagnetism is credited to the distance-dependent magnetic interaction between the two Co ions.

Acknowledgements

The authors would like to acknowledge the Defense Research and Development Organization (DRDO), India for providing the financial support (vide sanction letter no. ERIP/ER/0903766/M/01/1191) to carry out this work.

References

Archer P I, Santangelo S A and Gamelin D R 2007 *Nano Lett.* **7** 1037

Bartholomew D U, Suh E-K, Ramdas A K and Rodriguez S 1989 *Phys. Rev.* **B39** 5865

Bawendi M G, Carroll P J, Wilson W L and Brus L E 1992 *J. Chem. Phys.* **96** 946

Beaulac B R, Archer P I, Ochsenbein S T and Gamelin D R 2008 *Adv. Funct. Mater.* **18** 3873

Bruchez Jr M, Moronne M, Gin P, Weiss S and Alivisatos A P 1998 *Science* **281** 2013

Cullity B D 1978 *The elements of X-ray diffraction* (Reading, Massachusetts: Addison–Wesley) p. 102

Dietl T 2010 *Nature Mater.* **9** 965

Ekimov A I *et al* 1993 *J. Opt. Soc. Am.* **B10** 100

Furdyna J K 1982 *J. Appl. Phys.* **53** 7637

Furuseth S and Kjekshus A 1969 *J. Acta Chem. Scand.* **23** 2325

Hamdani F, Lascaray J P, Coquillat D, Bhattacharjee A K, Nawrocki M and Golacki Z 1992 *Phys. Rev.* **B45** 13298

Hanif K M, Meulenberg R W and Strouse G F 2002 *J. Am. Chem. Soc.* **124** 11495

Hasanzadeh J and Shayesteh S F 2011 *Optica Applicata* **XLI** 921

Hayashi A, Imada K, Inoue K, Ueda Y and Koji Kosuge K 1986 *Bull. Inst. Chem. Res., Kyoto Univ.* **64** 186

Hays J, Punnoose A, Baldner R, Engelhard M H, Peloquin J and Reddy K M 2005 *Phys. Rev.* **B72** 075203

Ikeda H, Shirai M, Suzuki N and Motizuki K 1995 *J. Magn. Mag. Mater.* **140** 159

Isber S, Christidis T, Tabbal M, Charar S and Goiran M 2001 *Physica* **B293** 304

Jin Y, Cui Q, Wang K, Hao J, Wang Q and Zhang J 2011 *J. Appl. Phys.* **109** 053521
Ladizhansky V, Faraggi A, Lyahovitskaya V and Vega S 1997 *Phys. Rev.* **B56** 6712
Lewicki A, Schindler A I, Furdyna J K and Giriat W 1989 *Phys. Rev.* **B40** 2379
Limaye M V, Singh S B, Das R, Poddar P and Kulkarni S K 2011 *J. Solid State Chem.* **184** 391
Meulenberg R W, Lee J R I, McCall S K, Hanif K M, Haskel D, Lang J C, Terminello L J and Buuren T V 2009 *J. Am. Chem. Soc.* **131** 6888
Murray C B, Norris D J and Bawendi M G 1993 *J. Am. Chem. Soc.* **115** 8706
Niu C-M, Kershaw R, Dwight K and Wold A 1989 *J. Solid State Chem.* **85** 262
Pearton S J, Heo W H, Ivill M, Norton D P and Steiner T 2004 *Semicond. Sci. Technol.* **19** R59
Peng X, Wickham J and Alivisatos A P 1998 *J. Am. Chem. Soc.* **120** 5343
Sambasivam S, Joseph D P, Lin J G and Venkateswaran C 2009 *J. Solid State Chem.* **182** 2598
Santara B, Pal B and Giri P K 2011 *J. Appl. Phys.* **110** 114322
Saravanan L, Pandurangan A and Jayavel R 2011 *J. Nanopart. Res.* **13** 1621
Seehra M S *et al* 2008 *Adv. Mater.* **20** 1656
Singh J and Verma N K 2012 *J. Supercond. Nov. Magn.* **25** 2425
Singh S B, Limaye M V, Date S K and Kulkarni S K 2008 *Chem. Phys. Lett.* **464** 208
Stroud R M, Hanbicki A T, Park Y D, Kioseoglou G, Petukhov A G and Jonker B T 2002 *Phys. Rev. Lett.* **89** 166602
Sundaresan A and Rao C N R 2009 *Nano Today* **4** 96
Toyosaki H, Fukumura T, Yamada Y, Nakajima K, Chikyow T, Hasegawa T, Koinuma H and Kawasaki M. 2004 *Nature Mater.* **3** 221
Wang Q, Pan D, Jiang S, Ji X, An L and Jiang B 2006 *J. Cryst. Growth* **286** 83
Williamson G K and Hall W H 1953 *Acta Metall.* **1** 22
Xu X, Xu C, Dai J, Hu J, Li F and Zhang S 2012 *J. Phys. Chem.* **C116** 8813
Yu J H *et al* 2010 *Nature Mater.* **9** 47
Zhang X, Zhang J, Zhao J, Pan B, Kong M, Chen J and Xie Y 2012 *J. Am. Chem. Soc.* **134** 11908